Label-free detection of DNA hybridization using carbon nanotube network field-effect transistors

Alexander Star*, Eugene Tu, Joseph Niemann, Jean-Christophe P. Gabriel, C. Steve Joiner†, and Christian Valcke‡

Nanomix, Inc., Emeryville, CA 94608

Edited by Mildred S. Dresselhaus, Massachusetts Institute of Technology, Cambridge, MA, and approved December 2, 2005 (received for review May 19, 2005)

We report carbon nanotube network field-effect transistors (NTNFETs) that function as selective detectors of DNA immobilization and hybridization. NTNFETs with immobilized synthetic oligonucleotides have been shown to specifically recognize target DNA sequences, including H63D single-nucleotide polymorphism (SNP) discrimination in the *HFE* gene, responsible for hereditary hemochromatosis. The electronic responses of NTNFETs upon single-stranded DNA immobilization and subsequent DNA hybridization events were confirmed by using fluorescence-labeled oligonucleotides and then were further explored for label-free DNA detection at picomolar to micromolar concentrations. We have also observed a strong effect of DNA counterions on the electronic response, thus suggesting a charge-based mechanism of DNA detection using NTNFET devices. Implementation of label-free electronic detection assays using NTNFETs constitutes an important step toward low-cost, low-complexity, highly sensitive and accurate molecular diagnostics.

hemochromatosis | SNP | biosensor

The development of nucleic acids diagnostics has become the subject of intense research, especially in the postgenome era. Current methods have mainly focused on optical detection using fluorescence-labeled oligonucleotides with dyes (1), quantum dots (2), or enhanced absorption of light by oligonucleotide-modified gold nanoparticles (3). On the other hand, label-free electronic methods promise to offer sensitivity, selectivity, and low cost for the detection of DNA hybridization (4). For example, microfabricated silicon field-effect sensors can monitor directly the increase in surface charge when DNA was hybridized on the sensor surface (5). Nanomaterials possess unique properties that are amenable to biosensor applications; they are one-dimensional structures that are extremely sensitive to electronic perturbations, readily functionalized with biorecognition layers, and compatible with many semiconducting manufacturing processes. Thus, one-dimensional silicon nanowires (6–8) and indium oxide nanowires (9) have shown promising performance, because their electronic conductance is more sensitive to DNA-associated charges as a result of their high surface-to-volume ratio. Using smaller nanowires with virtually all atoms on their surface, such as single-walled carbon nanotubes (SWNTs), will provide additional advantages in DNA detection. To date, there are several reports on electrochemical detection of DNA hybridization using multi-walled carbon nanotube electrodes (ref. 10 and references therein, and ref. 11). Whereas electrochemical methods rely on electrochemical behavior of the labels, measurement of direct electron transfer between SWNTs and DNA molecules paves the way for label-free DNA detection. SWNT-based field-effect transistors (12) have excellent operating characteristics (13), and they have already been explored for highly sensitive electronic detection of gases (14, 15) and biomolecules such as antibodies (16, 17).

Single-stranded DNA (ssDNA) has been recently demonstrated to interact noncovalently with SWNTs (18, 19). The ssDNA forms a stable complex with individual SWNTs by wrapping around them by means of the aromatic interactions between nucleotide bases and SWNT sidewalls. Double-stranded DNA molecules have also been proposed to interact with SWNTs as major groove binders (20). Here, we employ carbon nanotube network field-effect transistor (NTNFET) devices to investigate interactions between ssDNA oligonucleotides and SWNTs and subsequent DNA hybridization processes that take place on the device surface. We have found that NTNFETs can be selectively functionalized with DNA oligonucleotides and retain hybridization specificity. Thus, NTNFETs with immobilized synthetic oligonucleotides have been demonstrated to selectively recognize target DNA sequences with SNP. We demonstrate the single base mismatch discrimination using wild-type versus H63D mutation in the *HFE* gene, responsible for hereditary hemochromatosis.

Results and Discussion

DNA Immobilization and Hybridization on NTNFETs. First, we consider deposition of ssDNA on NTNFET devices. As a capture probe, ssDNA: 5′-CCT AAT AAC AAT-3′ (Alpha DNA) was selected. This oligonucleotide sequence was previously used in sensors based on silicon nanowires (8). Fig. 1*A* shows a fluorescent image of the interdigitated device with distance between electrodes of 10 μm after incubation with Cy5-labeled ssDNA capture probe, followed by thorough washings to remove excess and weakly bound DNA molecules. Whereas bare NTNFET devices have shown no measurable fluorescence signal (image is not shown), the devices after incubation with Cy5-labeled ssDNA show clear fluorescence (Fig. 1*A*). Interestingly, fluorescence clearly comes from device areas covered with carbon nanotubes; there is no fluorescence from the bare silicon surface. This observation supports selective adsorption of ssDNA molecules on the sidewalls of carbon nanotubes. The DNA incubation experiments were repeated under *the same conditions* with unlabeled ssDNA capture probe (Fig. 1*B*), to prepare the NTNFET devices for subsequent hybridization experiments with FITC-labeled complementary DNA sequences (Table 1). For fluorescent experiments, we used 50 nM target DNA to allow integration of the fluorescence signal in 10–20 sec to minimize photobleaching. The changes in fluorescence before (Fig. 1*B*) and after (Fig. 1*C*) hybridization confirm that DNA hybridization takes place under these experimental conditions.

Series of control experiments have been conducted to verify these observations. Fig. 1*D* shows fluorescent image of the NTNFET device after incubation with Cy5-labeled dA_{12} oligonucleotide. This ssDNA is adsorbed on carbon nanotubes in a

Conflict of interest statement: No conflicts declared.

This paper was submitted directly (Track II) to the PNAS office.

Abbreviations: NTNFET, carbon nanotube network field-effect transistor; PB, phosphate buffer; SWNT, single-walled carbon nanotube.

*To whom correspondence may be sent at the present address: Department of Chemistry, University of Pittsburgh, Pittsburgh, PA 15260. E-mail: astar@pitt.edu.

†Present address: Department of Chemistry and Biochemistry, University of California, Los Angeles, CA 90095.

‡To whom correspondence may be addressed. E-mail: cvalcke@nano.com.

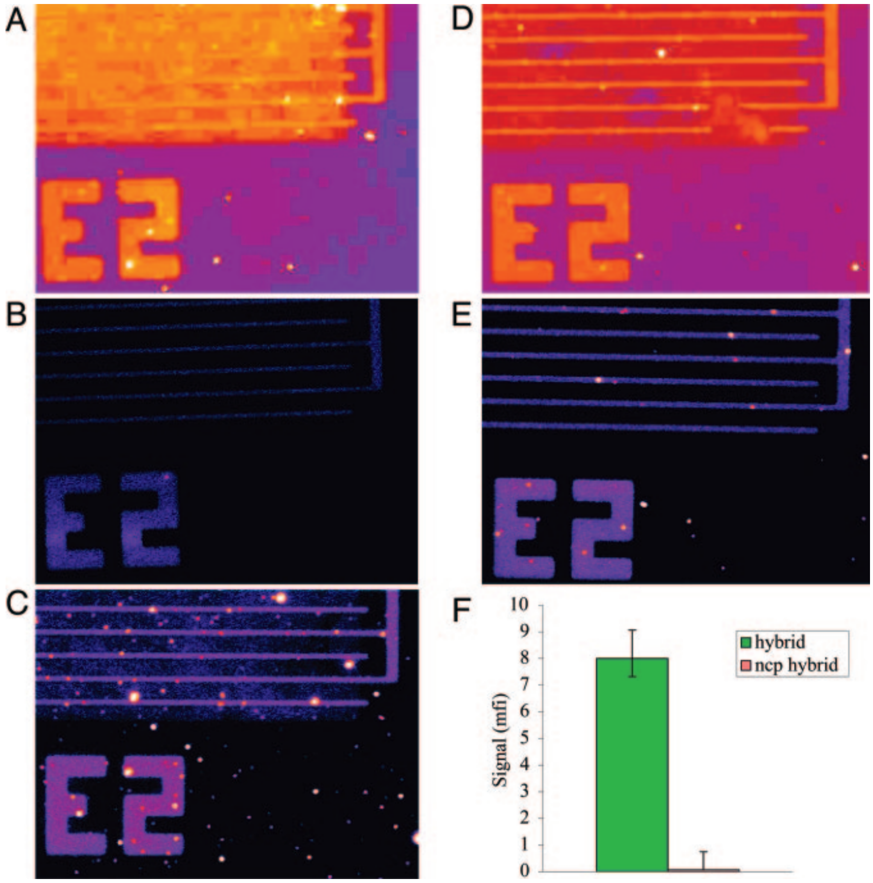

Fig. 1. Fluorescence microscopy images of the NTNFET devices with distance between electrodes of 10 μm after DNA incubations for 1 h followed by removing unbound DNA oligomers. Images after incubation with Cy5-labeled (*A*) and unlabeled (*B*) 12-mer oligonucleotide capture probes (5′-CCT AAT AAC AAT-3′). (*C*) The device with the unlabeled DNA capture probes after incubation with FITC-labeled complementary DNA target (5′ Fitc-ATT GTT ATT AGG-3′). Another set of experiments included dA_{12} as a capture DNA probe. (*D*) Image after incubation with Cy5-labeled A_{12} captures. (*E*) The device after incubation with the FITC-labeled DNA targets, which have homology with only six bases in dA_{12} captures. (Image before the target incubation is not shown.) (*F*) The graph associated with *C* and *E*. The fluorescent signals were measured as a difference between carbon nanotube device area and bare silicon wafer after a 20-sec integration.

similar fashion. Hybridization of a NTNFET device functionalized with unlabeled dA_{12} (fluorescent image is not shown) with the same DNA target resulted in significantly lower fluorescence (Fig. 1*E*). Quantitative comparison of target DNA hybridization, calculated as a difference between fluorescence signal from carbon nanotube area versus bare Si surface, have shown two orders of magnitude stronger signal for a DNA hybridization system containing fully matched DNA as opposed to a system containing mismatched DNA oligonucleotides (Fig. 1*F*). (There is only six-base homology between dA_{12} and the target DNA sequence.)

Next, we consider NTNFET device electronic responses for DNA immobilization and hybridization. Transistor characteristics such as G–V_g transfer curves, i.e., source-drain conductance

Table 1. Synthetic oligonucleotides used in fluorescent and electronic detection assays

	Sequence (5′ → 3′)
Capture probes	CCT AAT AAC AAT
	Cy5-CCT AAT AAC AAT
	AAA AAA AAA AAA
	Cy5-AAA AAA AAA AAA
Targets	FITC-ATT GTT ATT AGG
	ATT GTT ATT AGG

(G) as a function of applied gate voltage (V_g), are known to be sensitive to changes in environment around carbon nanotubes, including molecular presence (14). Although NTNFET devices used in this study had different absolute conductances, G–V_g characteristics such as modulation and threshold voltages were similar. Transfer characteristics of bare NTNFET devices are well described in the literature and consistent with *p*-type with positive threshold voltages (21). Incubation of the device with ssDNA capture probe on the device results in a shift of G–V_g curve toward more negative gate voltage values (Fig. 2). Interestingly, using dA_{12} oligonucleotide sequence as alternative capture probe results in similar shift of threshold voltage. It should be noted at this point that selective adsorption of ssDNA on device areas with SWNTs under this incubation/washing conditions was verified by fluorescent imaging. (We have observed similar shifts for both unlabeled and fluorescence labeled ssDNA sequences.) Based on these results, we may assume that ssDNA adsorbed on sidewalls of carbon nanotubes and results in electron doping to the carbon nanotube semiconductor channels of NTNFET. This change in NTNFET characteristics is similar to the effect observed for aromatic compounds, such as toluene (22). Aromatic nucleotide bases in ssDNA molecules may be exposed to form π-stacking interactions with the sidewalls of SWNTs. We find these results to be in total agreement with molecular modeling and experimental studies of DNA interaction with carbon nanotubes (18).

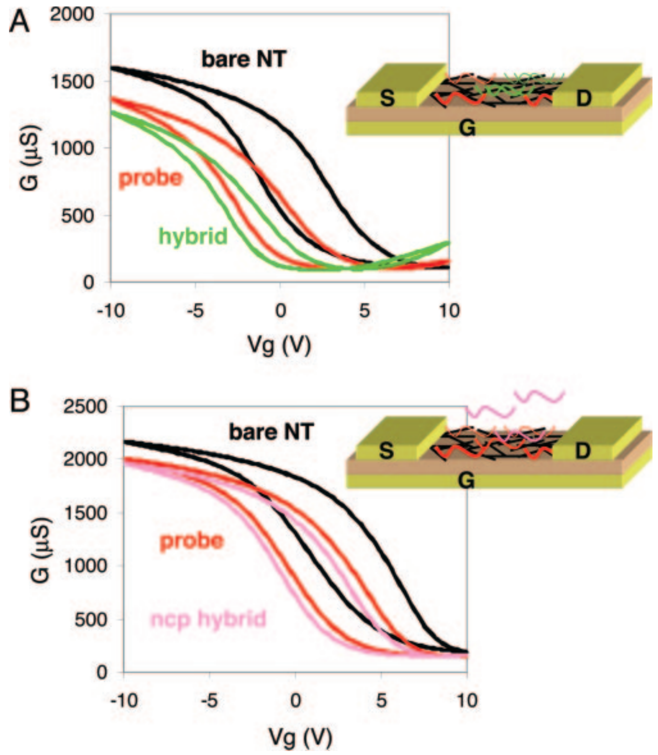

Fig. 2. Electronic measurements such as source-drain conductance (*G*) as function of gate voltage (V_g), and schematic drawings of the NTNFET devices used for DNA assays. (*A*) Before (bare NT) and after incubation with 12-mer oligonucleotide capture probes (5′-CCT AAT AAC AAT-3′), as well as after incubation with the complementary FITC-labeled DNA targets. (*B*) Before and after incubation with dA_{12} captures as well as after incubation with the DNA targets.

Furthermore, DNA hybridization experiments were investigated by NTNFET electronic measurements. DNA hybridization experiments with complementary target DNA sequence result in reduction of NTNFET conductance (Fig. 2*A*). There is significantly smaller change in device conductance in the system containing mismatched DNA oligonucleotides compared with fully matched DNA (Fig. 2*B*).

Hemochromatosis SNP Discrimination. To illustrate the practical utility of this nanoelectronic detection method, we present an allele-specific assay to detect the presence of SNP using NTNFETs. SNPs are the most abundant and highly conserved variations in the human genome and have been associated with a wide variety of diseases. The screening of large populations necessitates cost-effective and efficient high-throughput scanning, which will be facilitated by electronic and label-free techniques. We chose the H63D polymorphism in the human *HFE* gene that is associated with hereditary hemochromatosis, a common, easily treated disease of iron metabolism (23, 24).

NTNFET devices were applied to differentiate between mutant (*mut*) and wild-type (*wt*) alleles (Table 2). In two detection assays, NTNFET devices were functionalized by adsorption of either *wt* or *mut* 17-mer alleles. Hybridization of a long allele (51-mer) that includes the target sequence was conducted on these two chips. DNA hybridization in *wt*–*wt* matching combination, which was stable to our washing conditions, resulted in significant decrease of the device conductance (Fig. 3*A*). On the other hand, single-base mismatch combination between *mut* capture probe and *wt* target was not stable toward the washing conditions and resulted in significantly smaller change in the device characteristics (Fig. 3*B*). SNP discrimination was achieved at relative low stringency conditions: ≈25°C below melting temperature for this sequence, T_m = 46°C. Because target alleles were fluorescently labeled, the electronic measurements have been confirmed by fluorescent imaging. Fig. 3*C* summarizes both electronic and optical responses for hemochromatosis detection. For electronic responses, data from three devices with similar geometry and 10-μm pitch were calculated. We have plotted in Fig. 3*C* mean normalized response values and have added standard deviation error bars for those devices. Other devices on the chip have demonstrated similar trends in their responses and show that devices with 10-μm electrode pitch yields the best signal-to-noise ratio. Larger-pitch devices trended toward increased noise or were below the percolation threshold, whereas smaller-pitch devices exhibited poor modulation (Fig. 6, which is published as supporting information on the PNAS web site). These results clearly demonstrate that NTNFET device characteristics, such as maximum conductance or threshold voltage (data not shown), produce sensor results that are comparable to state-of-the-art optical technique.

Table 2. Synthetic *HFE* target mimics

	Sequence (5′ → 3′)
Allele-specific capture probes	
Wild type	TCT ATG AT**C** ATG AGA GT
Mutant	TCT ATG AT**G** ATG AGA GT
Synthetic *HFE* target	
Wild type	Cy5-ACG GCG ACT CTC AT**G** ATC ATA GAA CAC GAA CAG CTG GTC ATC CAC GTA GCC

Boldface type indicates site of polymorphism. Regions complementary to the capture probes are underlined.

Assay reproducibility and selectivity were tested in the presence of nonhomologous DNA to increase sample complexity. Chips were prepared with allele-specific capture probes as described above and hybridized with 100 pM *wt* target containing 5 μg/ml denatured (100°C, 10 min) salmon sperm DNA. Initial experiments indicated that the NTNFET response due to hybridization was obscured by the nonhomologous DNA, suggesting nonspecific adsorption to the nanotubes or competitive displacement of the capture probes (Fig. 3*D*, no block). We addressed the former mechanism by blocking nonspecific binding sites (NSB) with 0.01% Triton X-100 in 400 mM phosphate buffer (PB). Triton is a nonionic surfactant containing an aliphatic chain and a hydrophilic PEG group (n = 9–10) and has been shown to reduce NSB on nanotubes (25). The chips were incubated with the Triton X-100 solution for 15 min at room temperature and washed as previously described. The Triton blocking step enabled SNP discrimination at 100 pM target in the presence of 10^4-fold molar excess of nonhomologous DNA (Fig. 3*D*, TX100 block). This result also demonstrates that adsorbed capture probes are able to withstand mild surfactants and are not readily displaced.

Label-free detection has several advantages including cost, time, and simplicity. Handheld field-ready devices as opposed to laboratory methods using labor-intensive labeling and sophisticated optical equipment will be enabled by this approach. Because electronic measurement using NTNFET devices involves molecular interactions between DNA molecules and sidewalls of carbon nanotubes, carbon nanotubes themselves function as labels. To investigate mechanism of the NTNFET electronic detection of DNA molecules, we have further explored hybridization of unlabeled 12-mer oligonucleotides (Table 1) at different DNA and salt concentrations.

DNA Titrations/Effect of Counterions. First we discuss effect of salts on DNA detection using NTNFET. DNA deposition from water

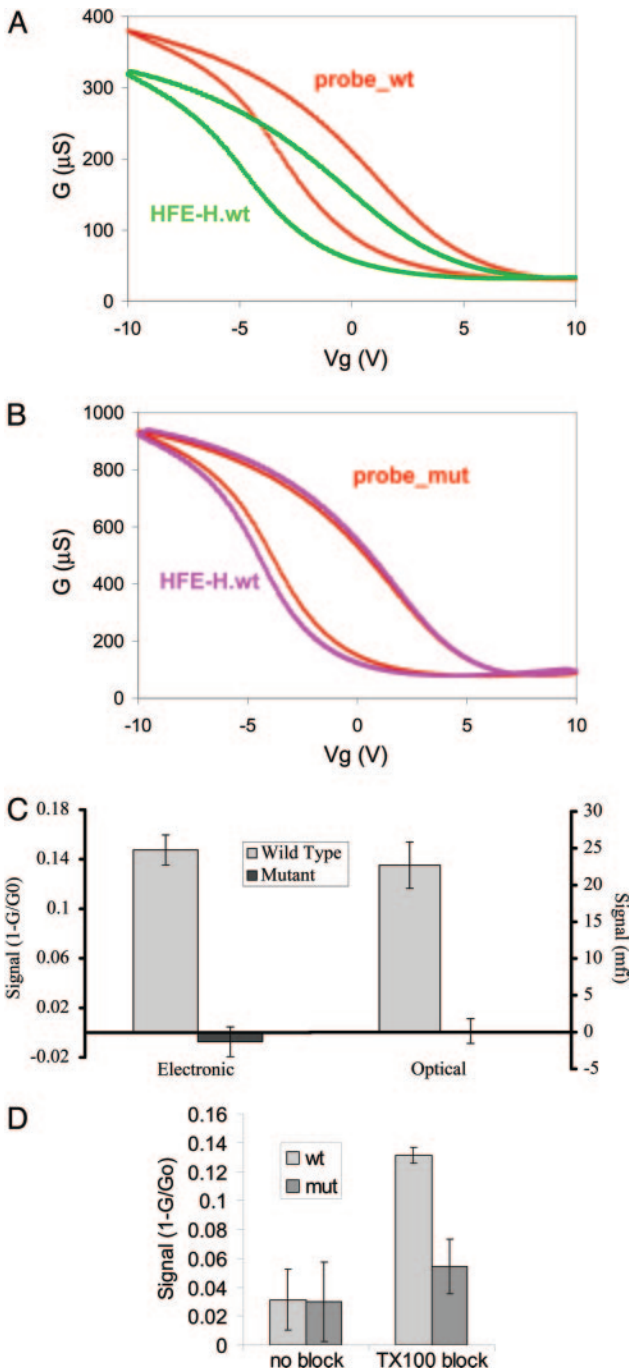

Fig. 3. Electronic detection of the presence of SNP in synthetic *HFE* amplicons. (*A*) G–V_g curves after incubation with allele-specific wild-type capture probe and after challenging the device with wild-type synthetic *HFE* target (50 nM). (*B*) G–V_g curves in the experiment with mutant capture probe. (*C*) Graph with electronic ($1 - G/G_0$) and fluorescent responses in SNP detection assays. For electronic response, average of normalized signals for three NTNFET devices were calculated. Error bars are equal to one standard deviation. (*D*) Graph with electronic ($1 - G/G_0$) responses in SNP detection assay ($n = 4$, $P = 0.002$) using 100 pM *wt* target in the presence of 5 μg/ml heat-denatured salmon DNA. no block, PB buffer; TX100 block, 0.01% Triton X-100 in PB buffer for 15 min at room temperature.

has shown similar change in the transfer characteristics (G–V_g) for deposition of ssDNA capture probe. However, hybridization experiments performed in water at 10 nM target DNA concentration have shown insignificant and unreproducible changes in G–V_g curve, resulting in either an increase or a decrease in device conductance.

We find that the presence of salts in DNA solution is needed to facilitate the hybridization and increase the change in NTNFET device characteristics. We have performed hybridizations with 1, 10, 50, 100, and 200 nM complementary DNA solutions in only PB buffer as well as with addition of $MgCl_2$ salt. Hybridizations with Mg^{2+} salt were also repeated at 1, 10, and 50 pM concentrations of complementary DNA (Fig. 4). After hybridization, we washed the NTNFET devices with the same salt concentrations (standard washing procedure). This step ensures that the observed changes in NTNFET device characteristics are not related to random changes in mobile charge concentrations on the device surface.

Although NTNFET devices used in this study had different conductances, G–V_g characteristics such as modulation and threshold voltages were similar. Plotting normalized values of maximum device conductance has demonstrated similar trends for different ranges of complementary DNA (target) concentrations. Two different NTNFET devices have close dependence, allowing treatment of data from two NTNFET devices in the same plot (Fig. 4*D*). It is tempting to attribute the difference in the slope value, which is almost factor of two, i.e., -0.11 for DNA (Na^+) versus -0.06 for both devices titrated with DNA (Mg^{2+}), to differences between single charge for monovalent sodium cation and double charge for divalent magnesium cation in DNA hybrid. These results are somewhat related to changes in NTNFET device characteristics when the devices were coated with Nafion electrolyte containing either monovalent (Na^+, K^+) or divalent (Ca^{2+}) ions (26).

We observed that the addition of Mg^{2+} during hybridization increased the sensitivity of DNA detection by 1,000-fold, from 1 nM to 1 pM, or from 5×10^9 to 5×10^6 molecules, compared with Na^+ alone. Furthermore, the dynamic range was increased from roughly 2.5 to 5 logs. Initially, we hypothesized that the observed differences were caused by the presence of more charge at the nanotube surface. Because of the experimental methodology and in particular standardized buffer washes, which were performed after each DNA incubation, NTNFET response to residual buffer or cation effects is negated. Moreover, we have conducted control experiments where the devices are hybridized in Na^+, and unbound target is washed away and then exposed to Mg^{2+}. Although replacement of Na^+ with Mg^{2+} had certain effects on the NTNFET response, the changes were significantly smaller compared with the presence of Mg^{2+} during hybridization (Fig. 7, which is published as supporting information on the PNAS web site). This observation leads us to conclude that Mg^{2+} increases the extent and overall efficiency of DNA hybridization on nanotubes. The dominant mechanism for improved sensitivity is driving the formation of DNA duplexes rather than the ionic species.

Conclusion

We have observed changes in NTNFET electronic characteristics that can be correlated with DNA detection. The results were confirmed by using fluorescently labeled DNA compounds that verified that DNA adsorption and hybridization were selective for nanotubes. Although sensors with only a few (and ideally with a single) carbon nanotube sensing elements can be fabricated (16), sensors used in this study contain a random network of nanotubes, covering a relatively large surface area between two metal electrodes (Fig. 5). The random network geometry has several advantages: it eliminates the problems of nanotube alignment and assembly, eliminates conductivity variations due to nanotube chirality and geometry, and is tolerant to individual SWNT channel failure because the device characteristics are averaged over a large number of nanotubes (27). In addition, such devices can be developed on low-cost flexible and/or

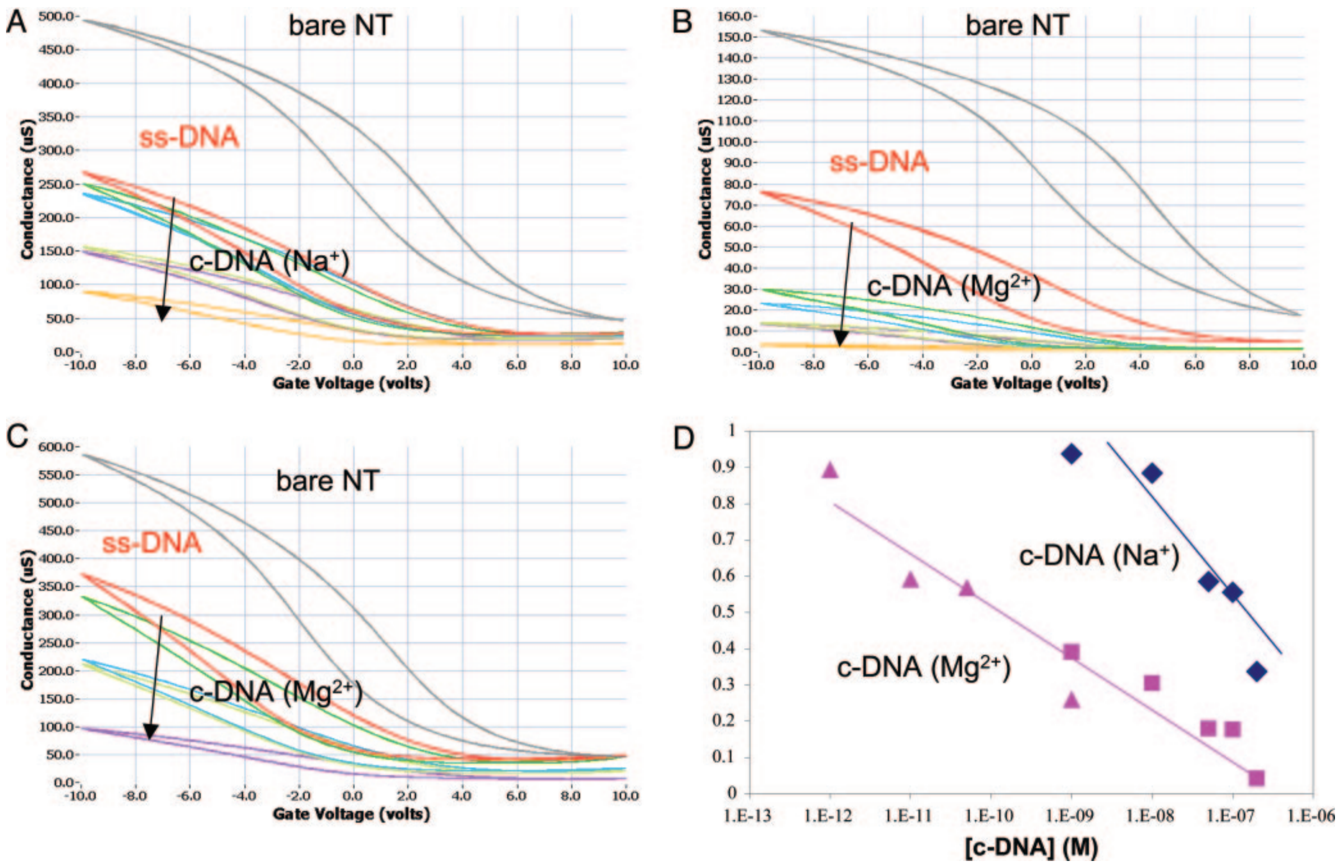

Fig. 4. Source-drain conductance (G) as function of gate voltage (V_g) of three NTNFET devices used for titration experiments with unlabeled oligonucleotides. (*A*) G–V_g curves before (bare) and after incubation with capture probe (ss-DNA) (5 μM in 200 mM PB, pH 7.2) as well as after incubations with target (c-DNA) (1, 10, 50, 100, and 200 nM in 200 mM PB). (*B*) As in *A*, except that incubations were conducted with target (c-DNA) (1, 10, 50, 100, and 200 nM in 10 mM PB/20 mM $MgCl_2$). (*C*) As in *A* but incubations with target (c-DNA) (1, 10, and 50 pM, and 1 nM in 10 mM PB/20 mM $MgCl_2$). (*D*) Plot of normalized conductance (G/G_0) of the three NTNFET devices as function of target DNA concentrations.

transparent polymer substrates by spray deposition or casting of nanotubes from solution (28).

In terms of sensitivity, SWNT may be superior if one considers it to be a true nanoscale sensor. Recently, Li *et al.* (29) compared metal oxide nanowires and NTNFETs and demonstrated comparable sensitivity for prostate-specific antigen. The limit of detection was ≈500 pg/ml or 14 pM at a signal-to-noise ratio of 2. As for intrinsic device characteristics, nanotubes exhibit surprisingly large electrical, or $1/f$, noise (30). The magnitude of the $1/f$ noise is inversely proportional to the number of charge carriers in the device, so a network with a large number of SWNTs reduces the $1/f$ noise by approximately the number of SWNTs raised to the (−1.3) power (31). For biodetection assays, the major noise sources are unclear and further study will be required to identify and quantify noise parameters. However, if $1/f$ noise is a significant factor, then large nanotube networks will have a distinct advantage over single-channel devices.

In summary, NTNFET devices have been used to investigate interactions of ssDNA with SWNTs as well as DNA hybridization processes. For example, electronic signal output from the NTNFET biochips clearly differentiated between mutant and wild-type alleles of the *HFE* gene, responsible for hereditary hemochromatosis. SNP discrimination was demonstrated in the presence of 5 μg/ml nonhomologous DNA, which approximates the concentration of DNA in a milliliter of blood. To make the NTNFET biochip detection platform more robust in whole-blood samples, certain modification to the sensor design will be required. For noncovalent approach, the use of longer capture probes or the addition of a

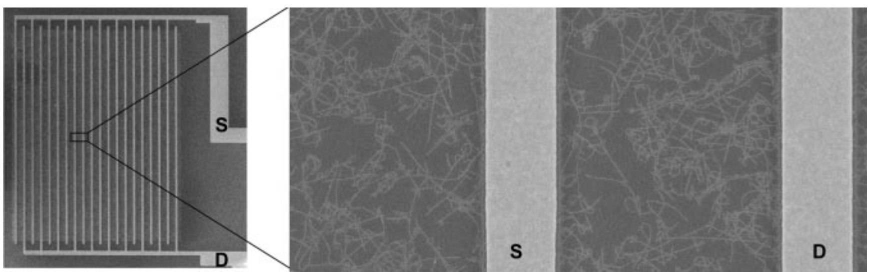

Fig. 5. Scanning electron microscopy image of the random network NTNFET device. The distance between source (S) and drain (D) interdigitated metal electrodes is 10 μm.

BIOPHYSICS

high-affinity linker sequence, such as the $(GT)_{20}$ oligonucleotide (18) or PEG, may make the attachment more robust in more complex samples. Covalent attachment of DNA capture probes may also improve the signal-to-noise ratio because surfactants can then be used to lower background (32). Moreover, microfluidics will be required to improve the sample-delivery method and allow manipulation of small volumes of DNA samples.

Materials and Methods

NTNFETs. Devices were fabricated by using SWNTs grown by means of chemical vapor deposition at 900°C using dispersed iron nanoparticles as growth promoter and a methane/hydrogen gas mixture on doped Si 100-mm wafers with SiO_2 at its surface. Electrical leads were patterned on top of the nanotubes from evaporated Ti-Au films (30- and 120-nm-thick, respectively) by using standard photolithography techniques. Each wafer consists of about 1,000 dies with 2.54 nm × 2.54-mm dimensions. On each die, a random network of SWNTs is patterned into several devices (210 μm × 270 μm) that consist of interdigitated electrodes with 10-μm separation (Fig. 5). Devices with other dimensions (pitches ranging from 5 to 100 μm) were also present on the die. Nanotubes outside the device area were removed by using oxygen plasma to electrically isolate each device. Electronic characterization of NTNFET devices, such as current flow between source and drain electrodes as a function of applied gate voltage and bias voltage, were conducted by using an autoprobe tester (Fig. 8, which is published as supporting information on the PNAS web site).

Data Acquisition. For DNA detection studies, chips with multiple NTNFET devices were wire-bonded and packaged in a 40-pin CERDIP and tested by using a NTNFET custom electronic test fixture, which measures an array of up to 12 separate sensors from each Si chip. The housing of the test fixture consists of a modified shielded I/O board (SCB-68; National Instruments) with a 40-pin ZIF socket. The I/O board was linked to a PC with a data acquisition card (PCI-6014; National Instruments). Programming to manage data acquisition was performed in LABVIEW (National Instruments). An analog output voltage was used to sweep the gate of the NTNFETs. Device characteristics such as source-drain voltage and current were calculated in LABVIEW from voltage measurements across sense resistors. Continuous I–V_g measurements were taken with a gate voltage triangle wave sweep at frequency of 3 Hz from −10 V to +10 V.

DNA Immobilization. Chemicals were purchased from Aldrich and used as received. Oligonucleotides unmodified and modified with Cy5 or FITC fluorescent labels at the 5′ end were synthesized by Alpha DNA. Allele-specific oligonucleotides for the H63D polymorphism study were synthesized by Integrated DNA Technologies. All DNA solutions were prepared by using 18-MΩ water (NANOpure Infinity UV water system; Barnstead). For DNA studies, packaged chips with NTNFET devices were cleaned in acid baths containing 0.1 M HNO_3, 0.1 M HCl, and 18-MΩ water on the orbital shaker for 15 min in each bath. As a standard washing procedure, the packages were rinsed by hand with 400 mM PB buffer (pH 7.2) and then washed two times in 400 mM PB on the orbital shaker for 5 min. The packages were then rinsed with 50 mM PB and blown dry with nitrogen before electronic testing.

For capture probe attachment to a NTNFET device, the chips were incubated in 5 μM solutions of oligonucleotides in 200 mM PB buffer for 1 h in a humid chamber. The standard washing procedure was then applied to remove excess and weakly bound DNA molecules before hybridization experiments. The hybridization experiments were performed by incubating the chips in 200 mM PB buffer solutions with complementary DNA (10 μl at 50 nM, unless otherwise noted) for 1 h in a humid chamber, followed by a standard washing procedure. All incubations were performed at room temperature (≈22°C).

Optical Imaging. Optical data were acquired by using a Zeiss Axioskop 40 microscope equipped with a thermoelectrically cooled monochromatic charge-coupled device camera (DVC). Cy5- and FITC-specific filter sets were obtained from Chroma Technology. Images were captured by using a Meteor II/digital frame grabber board and INTELLICAM software (Matrox). IMAGEJ was used for image processing and quantitation. The chips were imaged in 0.1 M sodium bicarbonate buffer (pH 8.3) to maximize FITC fluorescence emission.

We thank G. Grüner and R. G. Sosnowski for helpful discussions and the technical staff at Nanomix for their assistance with device fabrication and measurements. The sensor platform development was partially supported by National Science Foundation SBIR Grants 0450648 and 0340484. C.S.J. thanks the Materials Creation Training Program, NSF-IGERT, of University of California, Los Angeles, for summer internship support.

1. Pease, A. C., Solas, D., Sullivan, E. J., Cronin, M. T., Holmes, C. P. & Fodor, S. P. A. (1994) *Proc. Natl. Acad. Sci. USA* **91,** 5022–5026.
2. Gerion, D., Chen, F., Kannan, B., Fu, A., Parak, W. J., Chen, D. J., Majumdar, A. & Alivisatos, A. P. (2003) *Anal. Chem.* **75,** 4766–4772.
3. Taton, T. A., Mirkin, C. A. & Letsinger, R. L. (2000) *Science* **289,** 1757–1760.
4. Drummond, T. G., Hill, M. G. & Barton, J. K. (2003) *Nat. Biotechnol.* **21,** 1192–1199.
5. Fritz, J., Cooper, E. B., Gaudet, S., Sorger, P. K. & Manalis, S. R. (2002) *Proc. Natl. Acad. Sci. USA* **99,** 14142–14146.
6. Hahm, J. & Lieber, C. M. (2004) *Nano Lett.* **4,** 51–54.
7. Patolsky, F., Zheng, G. F., Hayden, O., Lakadamyali, M., Zhuang, X. W. & Lieber, C. M. (2004) *Proc. Natl. Acad. Sci. USA* **101,** 14017–14022.
8. Li, Z., Chen, Y., Li, X., Kamins, T. I., Nauka, K. & Williams, R. S. (2004) *Nano Lett.* **4,** 245–247.
9. Curreli, M., Li, C., Sun, Y., Lei, B., Gundersen, M. A., Thompson, M. E. & Zhou, C. (2005) *J. Am. Chem. Soc.* **127,** 6922–6923.
10. Wang, J. (2005) *Electroanalysis* **17,** 7–14.
11. Li, J., Ng, H. T., Cassell, A., Fan, W., Chen, H., Ye, Q., Koehne, J., Han, J. & Meyyappan, M. (2003) *Nano Lett.* **3,** 597–602.
12. Tans, S. J., Verschueren, A. R. M. & Dekker, C. (1998) *Nature* **393,** 49–52.
13. Avouris, Ph. (2002) *Acc. Chem. Res.* **35,** 1026–1034.
14. Kong, J., Franklin, N. R., Zhou, C., Chapline, M., Peng, S., Cho, K. & Dai, H. (2000) *Science* **287,** 622–625.
15. Collins, P. G., Bradley, K., Ishigami, M. & Zettl, A. (2000) *Science* **287,** 1801–1804.
16. Chen, R. J., Bangsaruntip, S., Drouvalakis, K. A., Wong Shi Kam, N., Shim, M., Li, Y., Kim, W., Utz, P. J. & Dai, H. (2003) *Proc. Natl. Acad. Sci. USA* **100,** 4984–4989.
17. Star, A., Gabriel, J.-C. P., Bradley, K. & Grüner, G. (2003) *Nano Lett.* **3,** 459–463.
18. Zheng, M., Jagota, A., Semke, E. D., Diner, B. A., Mclean, R. S., Lustig, S. R., Richardson, R. E. & Tassi, N. G. (2003) *Nat. Mater.* **2,** 338–342.
19. Zheng, M., Jagota, A., Strano, M. S., Santos, A. P., Barone, P., Chou, S. G., Diner, B. A., Dresselhaus, M. S., Mclean, R. S., Onoa, G. B., *et al.* (2003) *Science* **302,** 1545–1548.
20. Lu, G., Maragakis, P. & Kaxiras, E. (2005) *Nano Lett.* **5,** 897–900.
21. Snow, E. S., Novak, J. P., Campbell, P. M. & Park, D. (2003) *Appl. Phys. Lett.* **82,** 2145–2147.
22. Star, A., Han, T.-R., Gabriel, J.-C. P., Bradley, K. & Grüner, G. (2003) *Nano Lett.* **3,** 1421–1423.
23. Limdi, J. K. & Crampton, J. R. (2004) *Q. J. Med.* **97,** 315–324.
24. Franchini, M. & Veneri, D. (2005) *Ann. Hematol.* **84,** 347–352.
25. Shim, M., Kam N. W. S., Chen, R. J., Li, Y. & Dai, H. (2002) *Nano Lett.* **2,** 285–288.
26. Star, A., Han, T.-R., Joshi, V. & Stetter, J. R. (2004) *Electroanalysis* **16,** 108–112.
27. Rouhanizadeh, M., Tang, T., Li, C., Hwang, J., Zhou, C. & Hsiai, T. K. (2005) *Sensors Actuators B*, in press.
28. Bradley, K., Gabriel, J.-C. P. & Grüner, G. (2003) *Nano Lett.* **3,** 1353–1355.
29. Li, C., Curreli, M., Lin, H., Lei, B., Ishikawa, F. N., Datar, R., Cote, R. J., Thompson, M. E. & Chongwu, Z. (2005) *J. Am. Chem. Soc.* **127,** 12484–12485.
30. Collins, P. G., Fuhrer, M. S. & Zettl, A. (2000) *Appl. Phys. Lett.* **76,** 894–896.
31. Snow, E. S., Novak, J. P., Lay, M. D. & Perkins, F. K. (2004) *Appl. Phys. Lett.* **85,** 4172–4174.
32. Lee, C. S., Baker, S. E., Marcus, M. S., Yang, W. S., Eriksson, M. A. & Hamers, R. J. (2004) *Nano Lett.* **4,** 1713–1716.